PCCP

RSC Publishing

PAPER

View Article Online
View Journal | View Issue

Cite this: *Phys. Chem. Chem. Phys.*, 2013, **15**, 7370

Examination of the chemical behavior of the quercetin radical cation towards some bases†

Zoran Marković,*[a] Dragan Amić,[b] Dejan Milenković,[c] Jasmina M. Dimitrić-Marković[d] and Svetlana Marković[e]

Received 19th December 2012,
Accepted 18th March 2013

DOI: 10.1039/c3cp44605k

www.rsc.org/pccp

It has been generally accepted that, due to high ionization potential values, single electron transfer followed by proton transfer (SET-PT) is not a plausible mechanism of antioxidant action in flavonoids. In this paper the SET-PT mechanism of quercetin (Q) was examined by revealing possible reaction paths of the once formed quercetin radical cation ($Q^{+\bullet}$) at the M0-52X/6311+G(d,p) level of theory. The deprotonation of $Q^{+\bullet}$ was simulated by examining its chemical behavior in the presence of three bases: methylamine (representative of neutral bases), the MeS anion (CH_3S^-) and the hydroxide anion (representative of anionic bases). It was found that $Q^{+\bullet}$ will spontaneously be transformed into Q in the presence of bases whose HOMO energies are higher than the SOMO energy of $Q^{+\bullet}$ in a given medium, implying that Q cannot undergo the SET-PT mechanism in such an environment. In the reaction with the MeS anion in both gaseous and aqueous phases and the hydroxide anion in the gaseous phase $Q^{+\bullet}$ accepts an electron from the base, and so-formed Q undergoes the hydrogen atom transfer mechanism. On the other hand, SET-PT is a plausible mechanism of Q in the presence of bases whose HOMO energies are lower than the SOMO energy of $Q^{+\bullet}$ in a given medium. In such cases $Q^{+\bullet}$ spontaneously donates a proton to the base, with energetic stabilization of the system. Our investigation showed that Q conforms to the SET-PT mechanism in the presence of methylamine, in both gaseous and aqueous phases, and in the presence of the hydroxide anion, in the aqueous solution.

1 Introduction

To counteract the damaging effect of free radicals, the organisms rely on a variety of internal and external factors defying different defense mechanisms which prevent free radical damage. These factors include enzymes (such as superoxide dismutase and catalase), copper and iron transport proteins, water-soluble and lipid-soluble antioxidants and dietary substances, such as flavonoids, vitamins C and E, hydroquinones and various sulfhydryl compounds.[1]

Flavonoids are natural phenolic compounds recognized as potent external defense factors against oxidative damage. Their protective role correlates well with their antioxidant activity which is manifested through different actions, like direct radical scavenging, transition metal chelation, inhibition of certain enzymes, or removing oxidatively changed and damaged biomolecules. They can also manifest prooxidant, toxic effects involved in cytotoxicity, inhibition of mitochondrial respiration and mutagenicity, all closely related to their ability to oxidize in the presence of dissolved oxygen and to produce the superoxide anion which, in dismutation reaction, reacts with itself to produce oxygen and hydrogen peroxide which, through Fenton chemistry, gives a hydroxyl radical.[2–6]

Due to their electron-rich and highly conjugated chemical structure flavonoids easily participate in electron and proton transfers, the fundamental processes in chemistry and biology, which are also considered among the major determinants influencing good antioxidant activity. In the radical scavenging

[a] *Department of Chemical-Technological Sciences, State University of Novi Pazar, Vuka Karadžića bb, 36300 Novi Pazar, Serbia. E-mail: zmarkovic@np.ac.rs*
[b] *Faculty of Agriculture, The Josip Juraj Strossmayer University, P.O. Box 719, HR-31107 Osijek, Croatia. E-mail: damic@pfos.hr*
[c] *Bioengineering Research and Development Center, 6 Prvoslava Stojanovića, 34000 Kragujevac, Serbia. E-mail: deki82@kg.ac.rs*
[d] *Faculty of Physical Chemistry, University of Belgrade, 12-16 Studentski trg, 11000 Belgrade, Serbia. E-mail: markovich@ffh.bg.ac.rs*
[e] *Faculty of Science, University of Kragujevac, 12 Radoja Domanovića, 34000 Kragujevac, Serbia. E-mail: mark@kg.ac.rs*

† Electronic supplementary information (ESI) available: Tables listing the experimental and calculated geometrical parameters of Q and $Q^{+\bullet}$, plots of the HOMO of Q, NBO charges of Q and $Q^{+\bullet}$, the results of the IRC calculations for all TSs, tables presenting crucial bond distances of the participants in the examined reactions, spin density distribution of the participants in the investigated reactions, plots of ln *k versus* 1/*T* for all reactions of Q in the gaseous phase, and the energy profile for the reactions of the hydroxyl radical with different OH groups of Q in the gaseous phase. See DOI: 10.1039/c3cp44605k

mechanisms reactive radical species are inactivated by accepting a hydrogen atom from a hydroxyl group of the flavonoid. This transfer can be visualized through at least three mechanisms characteristic not only of flavonoids but phenolics generally: hydrogen atom transfer (HAT, eqn (1)), sequential proton loss electron transfer (SPLET, eqn (2)), and single electron transfer followed by proton transfer (SET-PT, eqn (3)).[7–15]

The HAT mechanism proceeds by rapid donation of a hydrogen atom to a radical species $R^{\bullet}$.

$$ArOH + R^{\bullet} \rightarrow ArO^{\bullet} + RH \quad (1)$$

The SPLET mechanism takes place once the flavonoid anion, ArO^{-}, is formed (eqn (2a)). Further, electron transfer from the flavonoid anion to a radical leads to the formation of the flavonoid radical, $ArO^{\bullet}$, and the corresponding anion R^{-} (eqn (2b)), which is further protonated (eqn (2c)).

$$ArOH \rightarrow ArO^{-} + H^{+} \quad (2a)$$

$$ArO^{-} + R^{\bullet} \rightarrow ArO^{\bullet} + R^{-} \quad (2b)$$

$$R^{-} + H^{+} \rightarrow RH \quad (2c)$$

The first step in the SET-PT mechanism is transfer of an electron to the radical form while the primary antioxidant, the flavonoid molecule, is transformed into the radical cation (eqn (3a)). It has been generally accepted that the second step proceeds through the flavonoid radical cation deprotonation (eqn (3b)).

$$ArOH + R^{\bullet} \rightarrow ArOH^{+\bullet} + R^{-} \quad (3a)$$

$$ArOH^{+\bullet} + R^{-} \rightarrow ArO^{\bullet} + RH \quad (3b)$$

Energetics related to radical scavenging mechanisms, which all have the same net result, are governed by different molecular properties: bond dissociation enthalpy (BDE) of ArOH in the HAT mechanism, proton affinity (PA) of ArO^{-} together with electron transfer energy (ETE) of ArO^{-} in the SPLET mechanism, and ionization potential (IP) of ArOH and proton dissociation enthalpy (PDE) of $ArOH^{+\bullet}$ in the SET-PT mechanism.

According to the structure–activity relationships, quercetin is consistently ranked as one of the most powerful antioxidants in the flavonoid class of compounds. Constant scientific interest in quercetin arises from its multiple effects on human health including: antiviral protection (against parainfluenza virus type 3, herpes simplex virus type 1, and poliovirus type 1), cardiovascular and anticancer protection, inhibition of oxidation of LDL cholesterol *in vitro*, inhibitory effects on inflammation-producing enzymes like cyclooxygenase and lipoxygenase which in their metabolic cycles cause edema, dermatitis, arthritis, gout and other pathological states. It is found as glycoside at high concentrations in many types of fruits and vegetables (*Ginkgo biloba*, *Hypericum perforatum*, *Sambucus canadensis*, apples, onion, berries, red wine, barks, nuts, flowers, leaves, seeds).[16–22] It has been shown that quercetin glucosides are hydrolyzed by lactase phlorizin hydrolase (LPH), a β-glucosidase found on the brush border membrane of the mammalian small intestine (pH = 7–9). Subsequently, the liberated aglycone can be absorbed across the small intestine.[23–25] Despite the fact that after absorption from the small intestine quercetin is conjugated with glucuronic acid or sulfate or *O*-methylation may occur,[24] the present study is focused on the SET-PT mechanism of aglycone of quercetin (Q) as a model compound representing these conjugates.

Besides reaction (3a) with electrophilic radicals, phenol radical cations can be generated in numerous ways. Phenol radical cations are potential intermediates in a number of photooxidative processes, and have been observed directly in matrices at low temperature,[26] and in gas-phase clusters.[27] It has been reported that photolysis of phenols leads to a variety of transients, including phenol radical cations.[28] In addition, it has been demonstrated that pulse radiolysis, photoionization, and laser flash photolysis can be used to generate and characterize a variety of phenol radical cations.[28,29] One can suppose that, when subjected to similar experimental conditions, Q can produce quercetin radical cation ($Q^{+\bullet}$). Our investigation is focused on reaction (3b), *i.e.* on possible reaction pathways *in vitro* of once formed $Q^{+\bullet}$ in a basic environment. The deprotonation of $Q^{+\bullet}$ was simulated by examining its chemical behavior in the presence of three bases: methylamine (representative of neutral bases), the MeS anion (CH_3S^{-}) and the hydroxide anion (representative of anionic bases). A general form of the investigated reactions is presented in Fig. 1. It will be shown that reaction (3b) plays a significant role in determining which mechanism of Q is dominant. Namely, the antioxidant mechanism of Q is directly dependent on the base charge and nature.

It should be pointed out that the structure of $Q^{+\bullet}$ has never been examined, probably due to the high IP value of Q in the gaseous phase. Though the IP and PDE values for some flavonoids have been reported,[30] the SET-PT mechanism of Q, and other flavonoids, has not been fully elucidated. The aim of this paper is to fulfil this gap in the quercetin chemistry.

2 Methodology section

All calculations were performed with the Gaussian 09 software package[31] using density functional theory. To select the suitable theoretical model, the geometry of Q in the gaseous phase was optimized using the M0-52X,[32–34] B3LYP,[35,36] B3P86, and PBE1PBE[37] functionals, with the 6-311+G(d,p) basis set (Tables S1 and S2, ESI†).

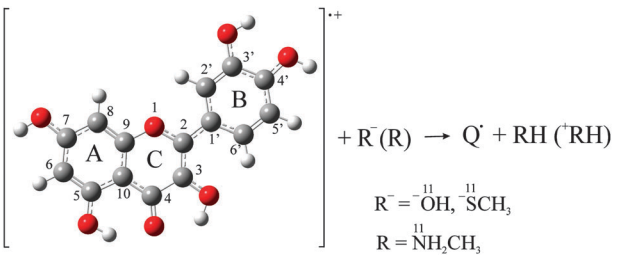

Fig. 1 General scheme of the examined reactions. The optimized structure represents the quercetin radical cation ($Q^{+\bullet}$), whereas $Q^{\bullet}$ stands for a quercetin radical. The labels on the atoms are remained throughout the paper.

A comparison to the experimental structure of Q shows that all methods well reproduce the bond lengths and angles of Q, with the mean relative errors of around 1.5%. On the other hand, only the M0-52X functional predicts the non-planar geometry of Q, in accord with the experimental τ(C3–C2–C1′–C2′) torsion angle (Table S1, ESI†). The performance of the M0-52X functional was further tested by applying the computationally more demanding cc-pvtz basis set (Tables S1 and S2, ESI†). As for the bond lengths and angles, the two basis sets produce almost identical mean relative errors, whereas 6-311+G(d,p) reproduces the τ(C3–C2–C1′–C2′) dihedral angle better than cc-pvtz. Taking into account all these facts, the M0-52X/6311+G(d,p) model was selected for all further calculations. Geometry optimizations for all species under investigation were achieved in the gaseous and aqueous phases, without symmetry constraints. The influence of water as solvent was approximated by the SMD solvation model.[38] SMD is a continuum solvation model based on the quantum mechanical charge density of a solute molecule interacting with a continuum description of the solvent. "D" in the model name stands for "density" to denote that the full solute electron density is used without defining partial atomic charges.

Transition states (TSs) were searched using synchronous transit guided quasi-Newton methods.[39] The intrinsic reaction coordinates (IRC), from the transition states down to the two lower energy structures, were traced using the IRC routine in Gaussian in order to verify that each saddle point is linked with the corresponding reactant complex (RC) and the product complex (PC).[40] The structure of RC for each reaction was obtained in the following way: the geometry which first results from progression backward along the reaction coordinate starting from the TS was selected, and then fully optimized without any movement restriction. Since each RC is treated as a single particle, the examined reactions can be considered as the first order reactions. Similarly, the structure of PC for each reaction was determined by selecting the geometry which first results from progression forward along the reaction coordinate, and then reoptimizing the selected geometry. The optimization and energy calculation of all geometries were performed without any constraints added to separate charges on the two moieties of RCs, TSs, and PCs. This implies that for each examined reaction, the global charge and spin multiplicity of the RC, TS and PC were mutually identical. The obtained geometries were verified, by normal mode analysis, to be minima (no imaginary frequencies), or maxima on the potential energy surface (one imaginary frequency). Natural bond orbital (NBO)[41–43] analysis was performed for all species.

Relative energies were calculated at 298 K. Zero point corrections (ZPE) and thermal corrections (TCE) to the energy were included. The M0-52X/6-311+G(d,p) values were corrected using the recommended scaling factor of 0.9467 for enthalpy and 0.9398 for entropy.[44]

Rate constants were calculated using conventional transition state theory (TST),[45–47] as implemented in TheRate program,[48] and the 1 M standard state as follows:

$$k = \sigma\kappa\frac{k_B T}{h}\exp(-\Delta G^{\ddagger}/RT) \quad (4)$$

where k_B and h stand for the Boltzman and Planck constants, $\Delta G^{\ddagger}$ is the free activation energy, σ represents the reaction path degeneracy accounting for the number of equivalent reaction paths, and κ accounts for tunneling corrections. The tunneling corrections, defined as the Boltzman average of the ratio between the quantum and classical probabilities, were calculated using the zero-curvature tunneling (ZCT) approach.[49,50] The energy values, partition functions, and thermodynamic data were taken from the quantum-mechanical calculations.

3 Results and discussion

Among several functionals and basis sets (see Methodology section) the M0-52X/6-311+G(d,p) model was selected. All results presented here were obtained at this level of theory. Reaction enthalpies related to the three mechanisms of free radical scavenging activity (HAT, SPLET, and SET-PT) of Q were calculated using the following equations:

$$\mathrm{BDE} = H(\mathrm{ArO}^{\bullet}) + H(\mathrm{H}) - H(\mathrm{ArOH}) \quad (5)$$

$$\mathrm{IP} = H(\mathrm{ArOH}^{\bullet+}) + H(\mathrm{e}^{-}) - H(\mathrm{ArOH}) \quad (6)$$

$$\mathrm{PDE} = H(\mathrm{ArO}^{\bullet}) + H(\mathrm{H}^{+}) - H(\mathrm{ArOH}^{\bullet+}) \quad (7)$$

$$\mathrm{PA} = H(\mathrm{ArO}^{-}) + H(\mathrm{H}^{+}) - H(\mathrm{ArOH}) \quad (8)$$

$$\mathrm{ETE} = H(\mathrm{ArO}^{\bullet}) + H(\mathrm{e}^{-}) - H(\mathrm{ArO}^{-}) \quad (9)$$

The species necessary to perform these calculations were generated from the most stable conformation of Q. Calculations were performed in the gaseous and aqueous phases (Table 1). The recommended values for the enthalpies in gas and water of electrons $H(\mathrm{e}^{-})$, hydrogen atoms $H(\mathrm{H})$, and protons $H(\mathrm{H}^{+})$ were used.[51–53] The results presented in Table 1 are in accord with the findings of a simultaneous investigation of the three mechanisms, *i.e.* HAT, SET-PT, and SPLET, for eight naturally occurring flavonoids (including Q).[30]

It can be concluded, on the basis of the BDE values, that among five OH groups of Q, the 4′-OH has the greatest ability to donate H-atom. The 4′-OH group has the lowest BDE value in both phases, so it represents the first site that can donate its H-atom, followed by 3-OH and 3′-OH.[54–56]

The calculated PA values of all present OH groups show that proton transfer from the 4′-OH group is easier compared to other OH groups. The PA values for aqueous solution are

Table 1 Parameters for free radical scavenging activity of quercetin (kJ mol^{-1}) calculated at the M05-2X/6-311G+(d,p) level of theory

	Gaseous phase					Aqueous solution				
	HAT	SPLET		SET-PT		HAT	SPLET		SET-PT	
Site	BDE	PA	ETE	IP	PDE	BDE	PA	ETE	IP	PDE
				737					334	
5	419	1422	318		1004	383	112	270		48
7	386	1363	345		971	383	94	289		49
3′	368	1429	261		953	349	116	232		14
3	355	1403	273		940	334	108	226		0
4′	319	1338	303		904	333	93	240		−1

several times lower than the corresponding values in the gaseous phase (Table 1), which is a consequence of the interactions of the species involved in eqn (2a) with the solvent molecules. This implies that the reaction which conforms to the SPLET mechanism is thermodynamically preferred in the aqueous solution.

The IP value of Q is significantly lower in the aqueous than in the gaseous phase, which is a consequence of the stabilization of charged species in polar solvents. It can be supposed that reaction (3a) will be faster in the aqueous solution, compared to the gaseous phase.[56,57]

Table 1 reveals that the HAT mechanism is dominant in the gaseous phase, because the BDE values are significantly lower than the corresponding IP and PA values. In the aqueous solution the PAs are significantly lower than the corresponding BDE values. This indicates that the SPLET mechanism represents the thermodynamically most probable reaction pathway in polar solvents. On the other hand, if we compare BDE to the sums PA + ETE (SPLET), and IP + PDE (SET-PT), it is clear that these values are mutually very similar. In other words, total energy requirements related to the SET-PT and SPLET mechanisms are equivalent to those of the HAT mechanism and are correlated perfectly with the BDE values. One can conclude, on the basis of these facts, that all three mechanisms are competitive in the aqueous solution. The BDE, PA and PDE values show that the 4′-OH group is the most reactive OH group of Q.

3.1 Electronic structure of the quercetin radical cation in the gaseous phase

Our calculations are in agreement with the experimental results that show that the B ring of Q deviates from planarity (Table S1, ESI†). This deviation can be attributed to the steric repulsion between O1 and H2′, and O3 and H6′, which is stronger than the effects of the weak hydrogen bonds (revealed by the NBO analysis) between these two pairs of atoms. The plot of the highest lying occupied molecular orbital of Q (Fig. S1, ESI†), whose energy is −0.26889 au, shows that the HOMO of Q is a delocalized π-like molecular orbital. It is reasonable to expect that, on excitation, the molecule of Q will lose an electron from this orbital, thus yielding the radical cation. The positive charge causes the shortening of the C–O bonds, in comparison to the parent molecule (Table S4, ESI†). Due to this fact, the O1–C2 and C3–O3 bonds become aromatic, which induces the aromatic nature of the C2–C3, C2–C1′, and C1′–C6′ bonds. Since the overlap among p orbitals is most successful in planar systems, the B ring of $Q^{+\bullet}$ lies in the plane of the A and C rings (Table S3, ESI†). The NBO analysis of $Q^{+\bullet}$ revealed the weak O3–H6′ hydrogen bond, resulting in the formation of the 6-membered ring of the pronounced aromaticity between the C and B rings, which additionally stabilizes the structure of $Q^{+\bullet}$. The aromaticity of the B ring and a part of the C ring enables $Q^{+\bullet}$ to delocalize its unpaired electron, and reduce the instability induced by the loss of an electron. The spin density map of $Q^{+\bullet}$ clearly reveals that the unpaired electron is delocalized over the C3, O3, C4′, and C6′ atoms (Fig. 2). The NBO analysis is in agreement with the spin density map, and shows that the spin

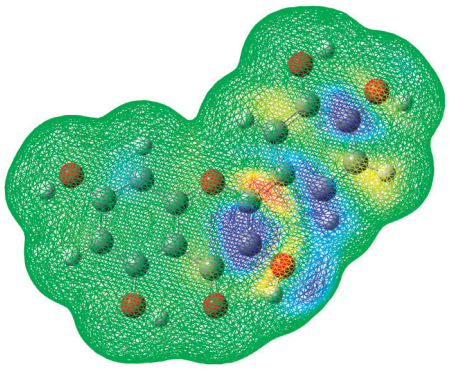

Fig. 2 Spin density map of $Q^{+\bullet}$. The blue regions indicate the highest spin density value.

density values on the C3, O3, C4′, and C6′ atoms amount to 0.31, 0.13, 0.18 and 0.14, respectively. The low spin density values of 0.07 and 0.06 were also observed on the C1′ and O4′ atoms. The highest spin density value on C3 can be attributed to the positive resonance effect of O3. This resonance effect is much stronger than that of O4′, since O4′ is involved in a relatively strong hydrogen bond with H3′ (the free energy of this hydrogen bond amounts to 16.1 kJ mol^{-1}).

The comparison of the charge distribution between Q and its radical cation is presented in Fig. S2 (ESI†). As expected, the oxygens of Q are particularly negatively charged, whereas hydrogens bonded to these oxygens are positively charged. The carbon atoms are partially negatively charged, except for those bonded to the oxygens, due to the negative inductive effect of these oxygens.

In $Q^{+\bullet}$ all carbon and oxygen atoms suffer either an increase of partial positive charge or reduction of partial negative charge. Since the unpaired electron is mostly delocalized over C3, O3, C4′, and C6′, these atoms exhibit a particular increase of partial positive charge or reduction of partial negative charge. Due to the increase of the partial charge on the oxygen and carbon atoms, the partial positive charges on the hydrogens in $Q^{+\bullet}$ are slightly decreased in comparison to the parent molecule.

3.2 Electronic structure of the quercetin radical cation in the aqueous solution

The water molecules form strong hydrogen bonds with the oxygen and hydrogen atoms of Q and $Q^{+\bullet}$, which leads to the elongation of the C–O and O–H bonds (Table S4, ESI†), and weakening of the intramolecular hydrogen bonds. The weakening of the O1–H2′ and O3–H6′ hydrogen bonds in Q leads to even larger deviation of the B ring from planarity (Table S3, ESI†). In the case of $Q^{+\bullet}$, the elongation of the O1–C2 and C3–O3 bonds leads to the lower aromaticity around the C2–C1′ bond. This fact, as well as the extremely weakened O3–H6′ hydrogen bond, explains the deviation of the B ring from planarity. In this way the steric repulsion between the O1–H2′ and O3–H6′ atoms is avoided.

Similarly to the case of the gaseous phase, the unpaired electron in the solvated $Q^{+\bullet}$ is distributed among the C3, O3,

C1′, C4′, O4′, and C6′ atoms. According to the NBO analysis, the spin density values for these atoms are as follows: 0.31, 0.13, 0.11, 0.19, 0.08, and 0.12, respectively.

3.3 Mechanism with the hydroxide anion in the gaseous phase

The reactions of the hydroxide anion with all OH groups of $Q^{+\bullet}$ were examined (Fig. 1). The transition states (TSs) for the reactions at positions 3, 3′, 4′, and 7 were revealed. As largely described, O4–H5 is a strong hydrogen bond, which is reflected in very high BDE, PA, and PDE values (Table 1).[10,54,58] For this reason, the reaction pathway at position 5 was not found out.

Inspection of the partial charges (Table 2) shows that O11 (Fig. 1) bears unexpectedly low partial negative charge in all reactant complexes (RCs). Actually, among all oxygens in each RC, O11 bears the lowest partial negative charge. Taking into account that O11 should belong to the hydroxide anion moiety, this finding is quite unusual. During the reaction course, the partial negative charge on O11 increases. The phenolic oxygens exhibit entirely opposite behavior, *i.e.* their partial negative charges decrease throughout the conversion of the RCs to the corresponding product complexes (PCs). The partial positive charges on phenolic hydrogens amount to around 0.5, with small variations during the reactions.

On the other hand, the spin density value on O11 is very close to unity in all RCs (Table 2), whereas the spin density values on all other atoms are practically equal to zero. These findings show that RCs consist of Q and hydroxyl radicals at different positions. Since the hydroxyl radical is electron deficient, the partial negative charge on O11 in RCs is significantly low. Why is the unpaired electron localized on O11? The hydroxide anion has two very high lying p orbitals where the lone pairs reside, whose energy (−0.02274 au) is higher than that of the SOMO of $Q^{+\bullet}$ (−0.41278 au). Thus, one of the HO^- electrons is spontaneously transferred to $Q^{+\bullet}$, yielding Q and hydroxyl radical. It is worth pointing out that the reaction $Q^{+\bullet} + HO^- \rightarrow Q + HO^\bullet$ is extremely exothermic (ΔG_r = −574.1 kJ mol^{-1}). In TSs the spin density is shared between O11 and the proximate phenolic oxygen (Table 2). Since all revealed TSs are early transition states, the spin density values on O11 are much larger. Finally, the spin density is distributed over the Q moiety, and its value on O11 is equal to zero in PCs. This finding shows that each PC consists of water molecules and the corresponding $Q^\bullet$. During the course of all reactions, the spin density on the phenolic hydrogens remains equal to zero. The spin density maps of the RC, TS, and PC for the reaction at position 4′ are presented in Fig. 3 as an illustration. In this PC the unpaired electron is delocalized over O4′, C3′, O3′, C5′, C1′, and C3, where the spin density values amount to 0.28, 0.24, 0.08, 0.15, 0.29, and 0.16, respectively.

All these facts clearly reveal that phenolic hydrogen is not transferred as a proton, but as an atom. Namely, reaction (3a), at least in the case where R^- = HO^-, is completely shifted to the left, implying that reaction (3b) does not occur at all. As expected, Q and hydroxyl radical conform to the HAT mechanism.[10,11]

The activation energies and rate constants at 298 K, as well as the reaction free energies for all hydrogen atom transfer reactions are presented in Table 3. Fig. S11–S14 (ESI†) clearly show that the tunneling effect is noticeable at low temperatures. With increasing temperature this effect rapidly decreases. These findings underline that tunneling effects are those responsible for making the reaction between quercetin and

Table 2 Partial charge and spin density values of the oxygens of interest. RC, TS and PC stand for the reactant complex, the transition state, and the product complex, respectively

		Partial charge			Spin density		
Site	Atom	RC	TS	PC	RC	TS	PC
7	O7	−0.689	−0.599	−0.546	0.00	0.25	0.36
	O11	−0.473	−0.642	−0.966	0.96	0.66	0.00
3′	O3′	−0.692	−0.669	−0.549	0.02	0.18	0.73
	O11	−0.415	−0.655	−0.958	1.01	0.73	0.00
3	O3	−0.697	−0.685	−0.563	0.00	0.18	0.33
	O11	−0.416	−0.641	−0.961	1.02	0.74	0.00
4′	O4′	−0.733	−0.723	−0.628	0.00	0.12	0.28
	O11	−0.474	−0.618	−0.970	0.96	0.78	0.00

Table 3 Thermochemical data for the investigated reactions. $\Delta G_a^{\ddagger}$, k^{TST}, k^{ZCT}, and ΔG_r denote activation free energy, rate constants (calculated by means of eqn (4) using the TST and ZCT approaches), and reaction free energy, respectively

Site	$\Delta G_a^{\ddagger}$ (kJ mol^{-1})	k^{TST} (M^{-1} s^{-1})	k^{ZCT} (M^{-1} s^{-1})	ΔG_r (kJ mol^{-1})
7	24.5	2.88×10^8	7.40×10^9	−98.7
3′	23.2	6.01×10^8	5.93×10^9	−128.6
3	23.1	7.46×10^8	3.69×10^{10}	−130.7
4′	13.0	4.22×10^{10}	2.28×10^{11}	−163.4

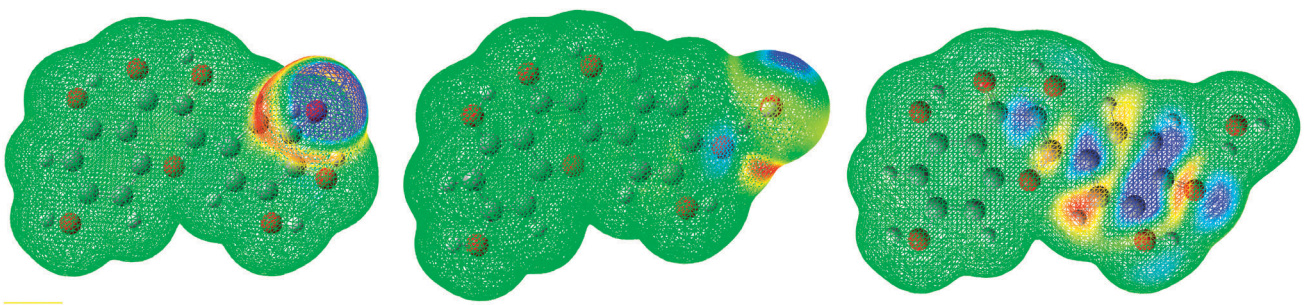

Fig. 3 Spin density maps of the reactant complex (left), the transition state (middle), and the product complex (right) for the H-atom transfer reaction at the position 4′.

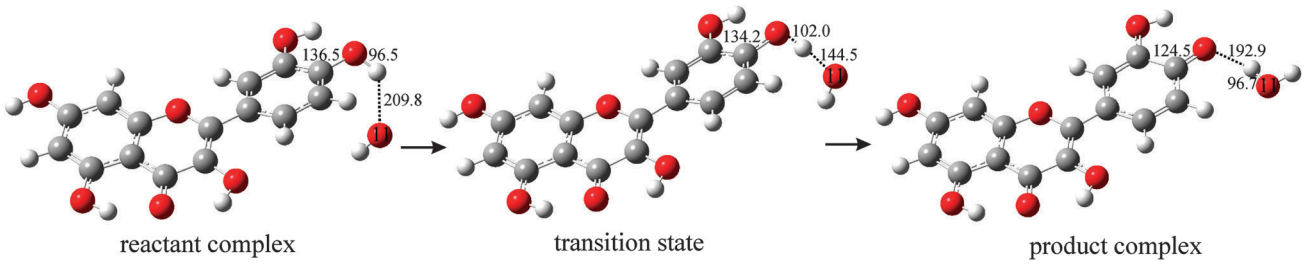

Fig. 4 Reaction path for the H-atom transfer from the 4′ position of quercetin to the hydroxyl radical. Selected bond distances are given in pm.

the OH radical faster. This behavior is to be expected, since the abstraction reaction involves the motion of a light particle (hydrogen atom) that can easily tunnel through the reaction barrier. As expected, the reactions are distinctly exothermic, while the activation energies are low, and corresponding rate constants are high. The O4′–H4′ homolytic bond cleavage requires the lowest activation energy (and shows the highest rate constant values), which can be attributed to the weakness of the O4′–H4′ bond, due to the involvement of O4′ in the relatively strong hydrogen bond with H3′. In addition, this reaction path yields the most stable PC. These findings are in accord with the results presented in Table 1, and with those obtained in the investigation of the reaction of Q with $^{\bullet}$OOH and $CH_3O^{\bullet}$ radicals.[10,11] The optimized geometries of the RC, TS, and PC for the most favorable hydrogen atom transfer reaction are depicted in Fig. 4.

3.4 Mechanism with the hydroxide anion in the aqueous solution

Transition states for the reactions of the hydroxide anion with phenolic groups at different positions of $Q^{+\bullet}$ in the aqueous solution were not revealed. On the other hand, our numerous attempts to optimize RCs led to the corresponding PCs, with the stabilization of the systems of −63.2, −67.8, −98.4, −114.7, and −121.1 kJ mol^{-1}, for the reactions at positions 5, 7, 3′, 3, and 4′, respectively. These facts indicate that, in the aqueous solution, phenolic hydrogen is spontaneously transferred to O11. To determine which mechanism is operative in the aqueous solution, it was assumed that the first structure which results from the optimization of a RC is most similar to the structure of the hypothetic RC in the aqueous solution. The NBO analysis for this structure, as well as for the corresponding PC, was performed. The results are summarized in Table 4. In each first structure O11 and corresponding phenolic hydrogen bear the largest negative and positive charges, and their spin density values are practically equal to zero. An inspection of the spin density values reveals that spin density is distributed over the Q moiety. These facts indicate that each RC consists of $Q^{+\bullet}$ and hydroxide anion. Due to the stabilization of the charged species in the polar solvent the energy of the degenerate HOMOs of the hydroxide anion (−0.31160 au) is lowered, whereas the energy of the SOMO of $Q^{+\bullet}$ is elevated (−0.29050 au), in comparison to the gaseous phase. Due to this fact, an electron is not spontaneously transferred from the hydroxide anion to $Q^{+\bullet}$. In the PCs the partial negative and positive charges on O11 and phenolic hydrogens are reduced in comparison to the first structure,

Table 4 The results of the NBO analysis for the reactions of hydroxide anion with $Q^{+\bullet}$ in the aqueous solution

	Charge			Spin density		
Structure	O5	H5	O11	O5	H5	O11
First	−0.755	0.536	−1.388	0.01	0.00	0.00
Product complex	−0.642	0.511	−1.023	0.25	0.00	0.00
	O7	H7	O11	O7	H7	O11
First	−0.730	0.541	−1.392	0.01	0.00	0.00
Product complex	−0.655	0.507	−1.025	0.26	0.00	0.00
	O3′	H3′	O11	O3′	H3′	O11
First	−0.694	0.547	−1.386	0.08	0.00	0.01
Product complex	−0.655	0.509	−1.025	0.31	0.00	0.00
	O3	H3	O11	O3	H3	O11
First	−0.629	0.526	−1.327	0.18	0.00	0.02
Product complex	−0.641	0.508	−1.024	0.30	0.00	0.00
	O4′	H4′	O11	O4′	H4′	O11
First	−0.692	0.559	−1.337	0.10	0.00	0.07
Product complex	−0.676	0.508	−1.025	0.26	0.00	0.00

whereas spin density is distributed in the manner exhibited by the corresponding $Q^{\bullet}$.[10] All these facts clearly show that phenolic hydrogens are transferred as protons, *i.e.*, that SET-PT is a plausible mechanism of Q in the aqueous solution. Thus, a significant increase of the spin density values on phenolic oxygens should be attributed to the loss of the protons.

In the text that follows the mechanisms of the reactions of $Q^{+\bullet}$ at the 4′ position with another anionic base, the MeS anion, and a neutral base, methylamine, will be presented.

3.5 Mechanism with the MeS anion

The energies of the HOMOs of the MeS anion in the gaseous and aqueous phases amount to −0.03088 and −0.21923 au, *i.e.* they are higher than the corresponding energies of the SOMOs of $Q^{+\bullet}$. In addition, the reaction $Q^{+\bullet} + CH_3S^{-} \rightarrow Q + CH_3S^{\bullet}$ is exothermic in both gaseous and aqueous phases (ΔG_r = −562.2 and −146.6 kJ mol^{-1}). On the basis of these facts, one can suppose that an electron from a lone pair of the MeS anion will spontaneously transfer to $Q^{+\bullet}$, and that the so formed Q will conform to the HAT mechanism, in both gaseous and aqueous phases.

This assumption was proved in a following manner: the reaction pathways in both gaseous and aqueous phases were revealed (Fig. 5). The reactions proceed *via* the TSs which

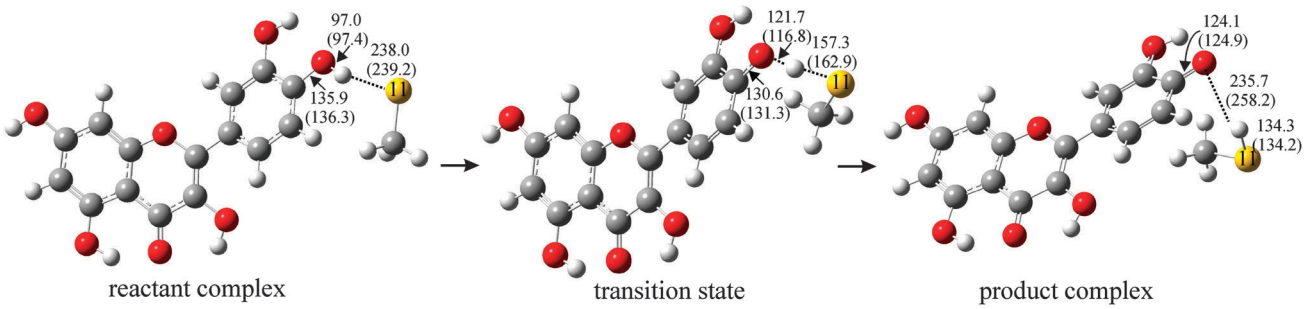

Fig. 5 Reaction path for the H-atom transfer from the 4′ position of quercetin to the $CH_3S^{\bullet}$ radical, with selected bond distances (pm). The values for bond distances in the aqueous solution are given in the brackets.

require the free activation energies of 44.2 kJ mol^{-1} (gaseous phase) and 61.0 kJ mol^{-1} (aqueous solution). The ΔG_r values amount to −20.1 kJ mol^{-1} (gaseous phase) and −11.4 kJ mol^{-1} (aqueous solution).

As expected, the spin density values in RC show that the unpaired electron is localized on S11 (Table 5). Since S11 is electron deficient, it bears partial positive charge. These facts undoubtedly show that RC consists of Q and $CH_3S^{\bullet}$ radical, which further undergo the HAT mechanism. Indeed, spin density is shared between S11 and the Q moiety in the TS. Finally, in PC, the spin density value on S11 is equal to zero, and the unpaired electron is delocalized over the Q moiety. As a consequence, S11 becomes partially negatively charged, whereas the partial negative charge on O4′ is reduced. The partial positive charge on H4′ decreases during the reaction, as it is transferred from more electronegative O4′ to less electronegative S11. These facts reveal that PC is composed of $Q^{\bullet}$ and CH_3SH molecule, and confirm that H4′ is transferred from Q to the $CH_3S^{\bullet}$ radical as an atom.

3.6 Mechanism with methylamine

The HOMO energy of CH_3NH_2 in the aqueous phase amounts to −0.31322 au, *i.e.* it is lower than the corresponding energy of the SOMO of $Q^{+\bullet}$. In the gaseous phase, the HOMO energy of CH_3NH_2 (−0.30685 au) is higher than the SOMO energy of $Q^{+\bullet}$, but the hypothetic reaction $Q^{+\bullet} + NH_2CH_3 \rightarrow Q + {}^{+\bullet}NH_2CH_3$ is endothermic (ΔG_r = 132.4 kJ mol^{-1}). The energetics of this hypothetic reaction is a consequence of the pronounced instability of the methylamine radical cation in comparison to the neutral parent molecule. On the basis of these facts, one can suppose that an electron from a lone pair of methylamine will not spontaneously transfer to $Q^{+\bullet}$, and that Q can undergo the SET-PT mechanism, in both gaseous and aqueous phases.

Table 5 Partial charge and spin density values of the atoms of interest. RC, TS and PC stand for the reactant complex, the transition state, and the product complex, respectively

	Partial charge			Spin density		
Atom	RC	TS	PC	RC	TS	PC
Gaseous phase						
O4′	−0.741	−0.671	−0.598	0.00	0.23	0.29
H4′	0.497	0.319	0.148	0.00	0.00	0.00
S11	0.132	−0.038	−0.071	0.98	0.42	0.00
Aqueous solution						
O4′	−0.755	−0.809	−0.663	0.00	0.04	0.28
H4′	0.512	0.361	0.145	0.00	0.00	0.00
S11	0.098	0.267	−0.102	0.97	0.90	0.00

Table 6 The results of the NBO analysis for the reaction of methylamine with $Q^{+\bullet}$ at the 4′ position

	Charge			Spin density		
Structure	O4′	H4′	N11	O4′	H4′	N11
Gaseous phase						
First	−0.666	0.521	−0.875	0.12	0.00	0.00
Product complex	−0.741	0.480	−0.733	0.20	0.00	0.00
Aqueous solution						
First	−0.657	0.554	−0.895	0.13	0.00	0.00
Product complex	−0.676	0.470	−0.704	0.26	0.00	0.00

The results for the reaction of $Q^{+\bullet}$ with methylamine in the gaseous and aqueous phases are mutually very similar. The reaction of spontaneous transfer of phenolic hydrogen to N11 occurs without an activation barrier, with the stabilization of the system of −72.6 kJ mol^{-1} (gaseous phase) and −77.6 kJ mol^{-1} (aqueous solution). To determine which mechanism is operative, the NBO analysis for the first structure which results from the optimization of the RC, as well as for the corresponding PC, was performed (Table 6).

In the first structure N11 and H4′ bear the largest negative and positive charges. Their spin density values are equal to zero, whereas the spin density is distributed over the Q moiety. These facts confirm that the RC consists of $Q^{+\bullet}$ and methylamine. In the PC the partial negative and positive charges on N11 and H4′ are reduced in comparison to the first structure, whereas spin density is distributed in the manner exhibited by the corresponding $Q^{\bullet}$.[10,11] All these facts clearly show that H4′ is transferred as a proton, *i.e.*, that Q conforms to the SET-PT mechanism in both gaseous and aqueous phases. Thus, an increase of the spin density value and the negative charge on O4′ should be attributed to the loss of the proton.

4 Conclusion

Antioxidant activity of flavonoids is usually examined by analyzing the thermodynamic properties of the parent molecules,

and the corresponding radicals, radical cations, and anions. According to this consideration, the IP values of flavonoids are notably high, especially in the gaseous phase.[10,11,54,58] For this reason, it has been generally accepted that SET-PT is not a plausible mechanism in flavonoids. In this paper the SET-PT mechanism of Q was examined by revealing possible reaction paths of $Q^{+\bullet}$ in a basic environment. For this purpose, the deprotonation of $Q^{+\bullet}$ was simulated by examining its chemical behavior in the presence of three different bases. Our investigations showed that, in spite of the much lower PDE value in comparison to the IP value (Table 1), reaction (3b) plays a crucial role in determining which mechanism of Q is dominant. The antioxidant mechanism of Q is directly dependent on the base nature and medium where the reaction of $Q^{+\bullet}$ occurs.

In the reaction of $Q^{+\bullet}$ with an anionic base, the MeS anion, in both gaseous and aqueous phases, an electron from a lone pair of the MeS anion spontaneously transfers to $Q^{+\bullet}$, thus yielding Q and $CH_3S^{\bullet}$ radical as RC. One can conclude that reaction (3a) is completely shifted to the left, implying that reaction (3b) will not occur at all. Instead, the formed RC undergoes the HAT mechanism.

On the other hand, once formed, $Q^{+\bullet}$ does not undergo the reverse reaction (3a) in the presence of methylamine in both gaseous and aqueous phases, implying that reaction (3b) is possible. Indeed, $Q^{+\bullet}$ spontaneously donates a proton to the base, with a stabilization of the system. These findings show that SET-PT is a plausible mechanism of Q with methylamine.

The reaction with the hydroxide anion lies in the middle of these two extremes. In the gaseous phase $Q^{+\bullet}$ and the hydroxide anion spontaneously transform into Q and hydroxyl radical, which further conform to the HAT mechanism.[10] Due to the stabilization of the charged species in polar solvents, Q can undergo the SET-PT mechanism in the presence of hydroxide anion in the aqueous solution.

Our final conclusion is as follows: whatever the source of $Q^{+\bullet}$ is, it will spontaneously be transformed into Q in the presence of bases whose HOMO energies are higher than the SOMO energy of $Q^{+\bullet}$ in a given medium, implying that Q cannot undergo the SET-PT mechanism in such an environment. On the other hand, SET-PT is a plausible mechanism of Q in the presence of bases whose HOMO energies are lower than the SOMO energy of $Q^{+\bullet}$ in a given medium.

Acknowledgements

This work was supported by the Ministry of Science of the Republic of Serbia (Projects No 172015 and 172016), Ministry of Science, Education and Sports of the Republic of Croatia (Project No 079-0000000-3211), Serbia–Croatia Bilateral agreement (69-00-74/2010-02), Croatia–Serbia Bilateral agreement (2011–2012), and Center for Scientific Research of the Serbian Academy of Sciences and Arts and University of Kragujevac.

References

1 B. Halliwell, R. Aeshbach, J. Loliger and O. Aruoma, *Food Chem. Toxicol.*, 1995, **33**, 601–617.
2 W. F. Hodnick, E. B. Milosavljevic, J. H. Nelson and R. S. Pardini, *Biochem. Pharmacol.*, 1998, **37**, 2607–2611.
3 R. H. Stadler, J. Markovic and R. Turesky, *Biol. Trace Elem. Res.*, 1995, **47**, 299–305.
4 W. F. Hodnick, F. S. Kung, W. J. Roettger, C. W. Bohmont and R. S. Pardini, *Biochem. Pharmacol.*, 1986, **35**, 2345–2357.
5 W. F. Hodnick, D. L. Duval and R. S. Pardini, *Biochem. Pharmacol.*, 1994, **47**, 573–580.
6 A. T. Cañada, E. Giannella, T. D. Nguyen and R. P. Mason, *Free Radicals Biol. Med.*, 1990, **9**, 441–449.
7 J. M. Mayer, D. A. Hrovat, J. L. Thomas and W. T. Borden, *J. Am. Chem. Soc.*, 2002, **124**, 11142–11147.
8 J. Mayer, *Annu. Rev. Phys. Chem.*, 2004, **55**, 363–390.
9 M. H. V. Huynh and J. Mayer, *Chem. Rev.*, 2007, **107**, 5004–5064.
10 Z. S. Marković, J. M. Dimitrić-Marković and Ć. B. Dolićanin, *Theor. Chem. Acc.*, 2010, **127**, 69–80.
11 S. G. Chiodo, M. Leopoldini, N. Russo and M. Toscano, *Phys. Chem. Chem. Phys.*, 2010, **12**, 7662–7670.
12 G. Litwinienko and K. U. Ingold, *Acc. Chem. Res.*, 2007, **40**, 222–230.
13 J. S. Wright, E. R. Johnson and G. A. DiLabio, *J. Am. Chem. Soc.*, 2001, **123**, 1173–1183.
14 E. Klein and V. Lukeš, *J. Phys. Chem. A*, 2006, **110**, 12312–12320.
15 G. A. DiLabio and K. U. Ingold, *J. Am. Chem. Soc.*, 2005, **127**, 6693–6699.
16 G. Cao, E. Sofic and R. L. Prior, *Free Radicals Biol. Med.*, 1997, **22**, 749–760.
17 C. A. Rice-Evans and N. J. Miller, *Biochem. Soc. Trans.*, 1996, **24**, 790–795.
18 B. Havsteen, *Biochem. Pharmacol.*, 1983, **32**, 1141–1148.
19 W. Bors, W. Heller, C. Michel and M. Saran, *Methods Enzymol.*, 1990, **186**, 343–355.
20 O. Benavente-Garcia, J. Castillo, F. R. Marin, A. Ortuño and J. A. Del Rio, *J. Agric. Food Chem.*, 1997, **45**, 4505–4515.
21 M. G. L. Hertog and P. C. H. Hollman, *Eur. J. Chem. Nutr.*, 1996, **50**, 63–71.
22 T. N. Kaul, E. Middleton Jr. and P. L. Ogra, *J. Med. Virol.*, 1985, **15**, 71–79.
23 A. J. Day, F. J. Cañada, J. C. Díaz, P. A. Kroon, R. Mclauchlan, C. B. Faulds, G. W. Plumb, M. R. A. Morgan and G. Williamson, *FEBS Lett.*, 2000, **468**, 166–170.
24 P. C. H. Hollman, *Pharm. Biol.*, 2004, **42**, 74–83.
25 F. A. van Dorsten, S. Peters, G. Gross, V. Gomez-Roldan, M. Klinkenberg, R. C. de Vos, E. E. Vaughan, J. P. van Duynhoven, S. Possemiers, T. van de Wiele and D. M. Jacobs, *J. Agric. Food Chem.*, 2012, **60**, 11331–11342.
26 Q. Sun, G. N. R. Tripathi and R. H. Schuler, *J. Phys. Chem.*, 1990, **94**, 6273–6277.
27 J. Steadman and J. A. Syage, *J. Am. Chem. Soc.*, 1991, **113**, 6786–6795.
28 O. Brede, H. Orthner, V. Zubarev and R. Hermann, *J. Phys. Chem.*, 1996, **100**, 7097–7105.
29 T. A. Gadosy, D. Shukla and L. J. Johnston, *J. Phys. Chem. A*, 1999, **103**, 8834–8839.
30 A. Vagánek, J. Rimarčík, V. Lukeš and E. Klein, *Comput. Theor. Chem.*, 2012, **991**, 192–200.

31 M. J. Frisch, G. W. Trucks, H. B. Schlegel, G. E. Scuseria, M. A. Robb, J. R. Cheeseman, G. Scalmani, V. Barone, B. Mennucci, G. A. Petersson, H. Nakatsuji, M. Caricato, X. Li, H. P. Hratchian, A. F. Izmaylov, J. Bloino, G. Zheng, J. L. Sonnenberg, M. Hada, M. Ehara, K. Toyota, R. Fukuda, J. Hasegawa, M. Ishida, T. Nakajima, Y. Honda, O. Kitao, H. Nakai, T. Vreven, J. A. Montgomery Jr., J. E. Peralta, F. Ogliaro, M. Bearpark, J. J. Heyd, E. Brothers, K. N. Kudin, V. N. Staroverov, R. Kobayashi, J. Normand, K. Raghavachari, A. Rendell, J. C. Burant, S. S. Iyengar, J. Tomasi, M. Cossi, N. Rega, J. M. Millam, M. Klene, J. E. Knox, J. B. Cross, V. Bakken, C. Adamo, J. Jaramillo, R. Gomperts, R. E. Stratmann, O. Yazyev, A. J. Austin, R. Cammi, C. Pomelli, J. Ochterski, R. L. Martin, K. Morokuma, V. G. Zakrzewski, G. A. Voth, P. Salvador, J. J. Dannenberg, S. Dapprich, A. D. Daniels, O. Farkas, J. B. Foresman, J. V. Ortiz, J. Cioslowski and D. J. Fox, *GAUSSIAN 09*, Wallingford, CT, 2009.
32 Y. Zhao and D. G. Truhlar, *Theor. Chem. Acc.*, 2008, **120**, 215–241.
33 Y. Zhao, N. E. Schultz and D. G. Truhlar, *J. Chem. Phys.*, 2005, **123**, 161103(1–4).
34 A. D. McLean and G. S. Chandler, *J. Chem. Phys.*, 1980, **72**, 5639–5648.
35 C. Lee, W. Yang and R. G. Parr, *Phys. Rev. B*, 1988, **37**, 785–789.
36 A. D. Becke, *J. Chem. Phys.*, 1993, **98**, 5648–5652.
37 J. P. Perdew, K. Burke and M. Ernzerhof, *Phys. Rev. Lett.*, 1996, **77**, 3865–3868.
38 A. V. Marenich, C. J. Cramer and D. G. Truhlar, *J. Phys. Chem. B*, 2009, **113**, 6378–6396.
39 C. Peng, P. Y. Ayala, H. B. Schlegel and M. J. Frisch, *J. Comput. Chem.*, 1996, **17**, 49–56.
40 C. Gonzalez and H. B. Schlegel, *J. Chem. Phys.*, 1989, **90**, 2154–2161.
41 J. E. Carpenter and F. Weinhold, *THEOCHEM*, 1988, **169**, 41–62.
42 E. D. Glendening, J. K. Badenhoop, A. E. Reed, J. E. Carpenter, J. A. Bohmann, C. M. Morales and F. Weinhold, *NBO 5.9; Theoretical Chemistry Institute*, University of Wisconsin, Madison, 2009.
43 A. E. Reed, L. A. Curtiss and F. Weinhold, *Chem. Rev.*, 1988, **88**, 899–926.
44 J. P. Merrick, D. Moran and L. Radom, *J. Phys. Chem.*, 2007, **111**, 11683–11700.
45 H. Eyring, *J. Chem. Phys.*, 1935, **3**, 107–115.
46 M. G. Evans and M. Polanyi, *Trans. Faraday Soc.*, 1935, **31**, 875–894.
47 D. G. Truhlar, W. L. Hase and J. T. Hynes, *J. Phys. Chem.*, 1983, **87**, 2664–2682.
48 W. T. Duncan, R. L. Bell and T. N. Truong, *J. Comput. Chem.*, 1998, **19**, 1039–1052.
49 C. Eckart, *Phys. Rev.*, 1930, **35**, 1303–1309.
50 R. A. Marcus, *Annu. Rev. Phys. Chem.*, 1964, **15**, 155–196.
51 J. E. Bartmess, *J. Phys. Chem.*, 1994, **98**, 6420–6424.
52 E. Klein, V. Lukeš and M. Iličin, *Chem. Phys.*, 2007, **336**, 51–57.
53 J. Rimarčik, V. Lukeš, E. Klein and M. Ilčin, *THEOCHEM*, 2010, **952**, 25–30.
54 M. Musialik, R. Kuzmicz, T. S. Pawlowski and G. Litwinienko, *J. Org. Chem.*, 2009, **74**, 2699–2709.
55 T. Kakiuchi, K. Mukai, K. Ohara and S. Nagaoka, *Bull. Chem. Soc. Jpn.*, 2009, **82**, 216–218.
56 Z. Marković, D. Milenković, J. Đorović, J. M. Dimitrić-Marković, V. Stepanić, B. Lučić and D. Amić, *Food Chem.*, 2012, **134**, 1754–1760.
57 C. Iuga, J. R. Alvarez-Idaboy and N. Russo, *J. Org. Chem.*, 2012, **77**, 3868–3877.
58 M. Leopoldini, T. Marino, N. Russo and M. Toscano, *Theor. Chem. Acc.*, 2004, **111**, 210–216.

